Australian Earthquake Engineering Society
2024 National Conference, 21-23 November 2024
Adelaide, South Australia

Statistical properties and modelled duration of an intracontinental earthquake sequence: 2021 M_W 5.9 Woods Point earthquake, Australia

Yunqi Huang[1], Mark Quigley[1], James La Greca[1] , Jake Wilcox[2], Elodie Borleis[2], Eleanor Green[1], Wayne Peck[2]

1. School of Geography, Earth, and Atmospheric Science, The University of Melbourne, Parkville, Australia

2. Seismology Research Center, 141 Palmer Street, Richmond VIC 3121 Australia

Abstract

We investigate the statistical properties of the 2021 moment magnitude (M_w) 5.9 Woods Point earthquake aftershock sequence (WPAS) in Victoria, Australia. WPAS Gutenberg-Richter b-values range from 0.76 to 1.07 and depend upon the earthquake magnitude type used (M_W vs M_L) and minimum completeness magnitude (Mc). The WPAS Modified Omori's law *p*-value of 0.83-0.84 suggests slower aftershock decay rates relative to the global average (e.g., p ≈ 1.1). The modelled duration of the WPAS (ca. 7 to more than 40 years) is consistent with analogous earthquakes globally. The high double-couple component (>80%) of the mainshock and strong statistical fit of a sub-vertical plane to the aftershock cloud favour a structurally simple mainshock source fault. However, the delayed occurrence of the largest aftershocks (M_L 4.7 occurred in June 2023, and M_L 4.2 occurred in August 2024) and a high proportion (~70%) of WPAS moment release sourced at distances > 1.5 km from the mainshock fault suggests aftershock activity on nearby structurally complex fault networks, as observed in other Australian sequences.

Keywords: Woods Point Earthquake, Intraplate Earthquake, Statistical Seismology.

1 Introduction

Aftershock sequences may be protracted in time and space and present numerous hazards to people, infrastructure, and landscapes (e.g., Quigley et al., 2016). In a typical earthquake sequence, the mainshock is associated with the largest seismic moment release (Shcherbakov & Turcotte, 2004) and the subsequent aftershocks (i.e., smaller-magnitude earthquakes in the time-and-space vicinity of the mainshock) may be triggered by a variety of static, dynamic, and post-seismic stress transfer mechanisms (Freed, 2005). The duration and behaviour of aftershock sequences may be influenced by the mainshock fault properties, crustal structure, tectonic setting, and other seismotectonic aspects (e.g., Stein & Liu, 2009; Ozawa & Ando, 2021). The apparent duration of aftershock sequences of specified magnitude ranges can range from days to several thousand years, and has been shown to be strongly positively correlated with mainshock magnitude and negatively correlated with background seismicity rates (Hainzl et al., 2016). Aftershock duration estimates and other seismic parameters (see

methods below) are relevant for probabilistic seismic hazard assessments (Toda & Stein, 2018) and operational earthquake forecasts (Jordan et al., 2011).

The 2021 M_W 5.9 Woods Point earthquake in Victoria, Australia, stimulated an aftershock sequence (Woods Point aftershock sequence; WPAS) that include several local magnitude (M_L) ≥ 4 earthquakes (Figure 1) (Ninis et al., 2021). To enhance our understanding of SCR aftershock sequences, we calculate the parameters of the Gutenberg-Richter (G-R) Law and Modified Omori's Law, model the duration of the WPAS, and compare the seismicity spatial distribution and monthly seismic moment release with the pre-mainshock background seismicity. Additionally, we model several rupture planes based on the spatial distribution of the WPAS to assess the distribution of aftershocks relative to the modelled mainshock source fault.

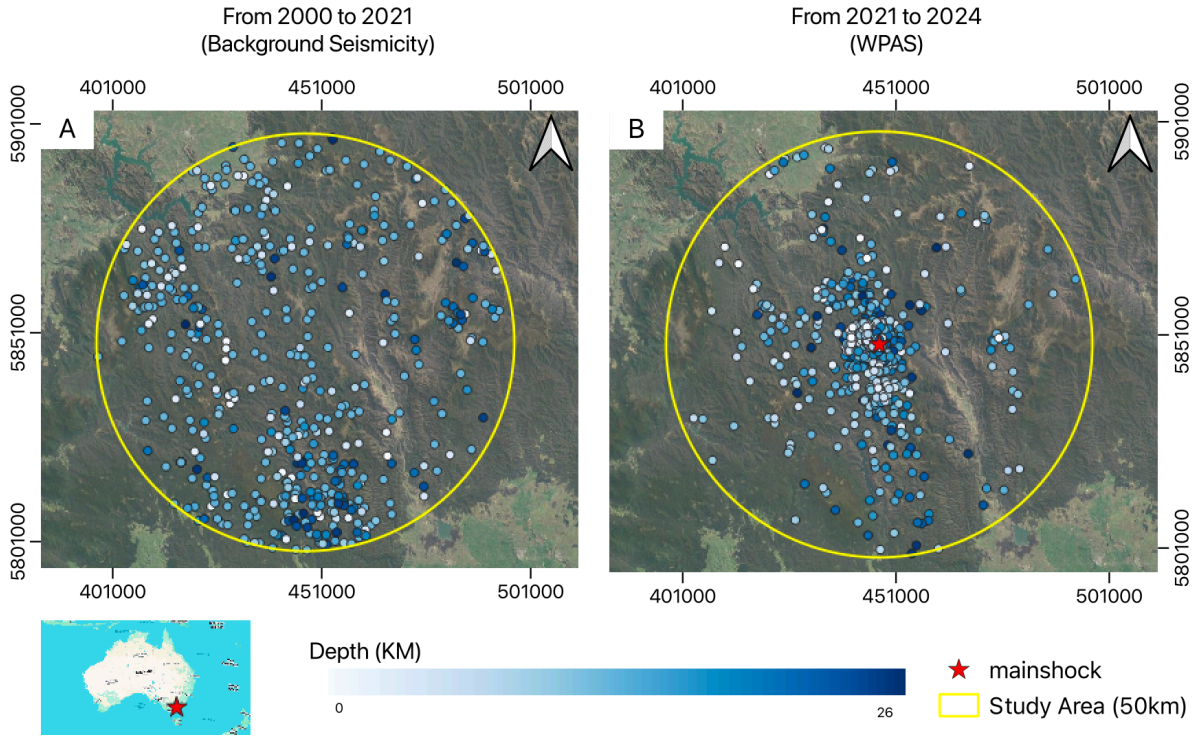

Figure 1. Location of seismicity observed in the WPAS region. Figure A displays the background seismicity recorded during the pre-mainshock stage (2000 to 2021) within a 50 km radius from the mainshock epicentre (-37.506°, 146.402°). Figure B shows the WPAS from 2021 to 2024 within the same spatial domain. The depths of the observed events are provided in kilometres below sea level (BSL). The surface elevation in the study area ranges from 350 to 1400 metres. Figures A and B use the EPSG:7855 projected coordinate system. Legend shows the location of the Woods Point M_W 5.9 mainshock. The source of observed seismicity is the Seismology Research Centre.

2 Data

The data was obtained from the Seismology Research Center (SRC) that incorporates information from a commercial seismometer network and data from Geoscience Australia (GA) and the United States Geological Survey (USGS). Notably, the dataset from SRC is not publicly accessible. For a detailed description, please refer to Appendix 1 at GitHub: https://github.com/Yunqi12/Data-Description-Methodology.

The networks deployed in Woods Point consist of a combination of The University of Melbourne (Unimelb) network and the SRC network. The SRC catalogue incorporates data from both networks to locate events. To enhance aftershock recording, ten temporary seismometers were deployed between 24 and 25 September and remained in the field for

several weeks to a couple of months. After initially locating the events, SRC manually relocated them using waveform analysis, maintaining a location uncertainty of 1-2 km.

SRC installed GA's instruments on 24 and 25 September, concurrent with the deployment of the Unimelb's instruments. The GA's instruments were removed by SRC on 10th and 11th February 2022. The instruments from Unimelb were incrementally removed from September 2021 to January 2022. With the full aftershock network deployed, computed epicentre uncertainties were generally less than 100-200 metres horizontally and approximately 100 metres more vertically. After the removal of GA's instruments, these uncertainties increased to approximately 300-500 metres horizontally and up to 800 metres to 1 km vertically. Before the aftershock network installation and following its removal, uncertainties were approximately 1-2 km horizontally and up to 3 km in depth. SRC used the VIC5A velocity model to calculate uncertainties in the Woods Point area by fitting arrival times to the model. However, as the seismicity model is one-dimensional, there is significant epistemic uncertainty about how accurately it reflects the "true" nature of seismic velocities in the region.

Select details of the datasets used in this study include:

Background Seismicity (2000 to 2021): The observed seismicity recorded within a 50 km radius from the mainshock epicentre (SRC location) from 2000 until the occurrence of the mainshock represents the background seismicity level during the pre-mainshock stage for the WPAS region in this study.

Synthetic Background Seismicity I: A synthetic seismicity model was developed based on Gutenberg-Richter Law parameters adjusted from long-term statistical results for southeastern Australia, tailored to our study area to address limitations in temporal and spatial coverage for comparison.

Synthetic Background Seismicity II: A synthetic seismicity model was developed based on the spatial distribution of background seismicity in the WPAS region from 2000 to 2021. Using the observed characteristics of this distribution (such as epicentre and depth distribution), a synthetic catalogue with 10,000 events was generated to represent the background seismicity during the pre-mainshock stage and to address limitations in the temporal sampling window. For detailed information on Synthetic Background Seismicity II, please refer to Appendix 3, available at https://github.com/Yunqi12/Data-Description-Methodology.

Regional Background Seismicity I: A seismicity model within the National Seismic Hazard Assessment 2023 (NSHA23, Allen et al., 2023) for the Eastern Australian Phanerozoic Accretionary Terranes, which covers most of the onshore area of eastern Australia, is used for comparison of Gutenberg-Richter Law b-value.

3 Methodology

The following methods are used in this research:

(i) Magnitude Completeness (Mc) Estimation: We used the Maximum Curvature (MAXC) method (Wyss et al., 1999; Wiemer & Wyss, 2000), the Mc Estimation Based on b-value Stability (MBS) method (Cao & Gao, 2002), and the bootstrapping method (Efron & Tibshirani, 1994) to calculate Mc for background seismicity and WPAS. **(ii) Gutenberg-Richter Analysis:** The Maximum Likelihood Estimation (MLE) method (Aki, 1965; Utsu, 1965) was used for b-value estimation, and the method by Shi & Bolt (1982) was employed for calculating b-value uncertainty. **(iii) Modified Omori's Law**: Parameters were estimated using the MLE method (Ogata, 1983) and Bayesian Analysis (Holschneider et al., 2012). **(iv) Fault Plane Fitting:** We applied the Linear Algebra and Coordinate Rotation methods for fault plane fitting. **(v) Aftershock Modelled Duration**: we used the Seismicity Spatial Distribution, Seismic Moment

Monthly Released, and Seismicity Rate methods to estimate. Full methodological details are available at GitHub: https://github.com/Yunqi12/Data-Description-Methodology

4 Results and Discussion

4.1 Gutenberg-Richter Law (G-R Law)

We calculated the a-value and b-value using three different methods to determine the Mc for the pre-mainshock mainshock background seismicity and the WPAS (Table 1), considering both magnitude types (M_L and M_W). The MAXC method often underestimates Mc (Wiemer & Wyss, 2000; Mignan & Woessner, 2012), while the MBS method, though more reliable for Mc selection, tends to overestimate it (Woessner & Wiemer, 2005; Mignan & Woessner, 2012). Both methods introduce sampling error due to limited time and space windows (Table 1). To mitigate this, we combined the bootstrapping method with both Mc estimation methods. The Mc values estimated by the MAXC and MBS methods fall within the uncertainty range of the MAXC+bootstrapping and MBS+bootstrapping methods respectively. However, there is a trade-off between using smaller Mc values (i.e., incorporating more earthquakes but reducing confidence in catalogue completeness) and larger Mc values (i.e., including fewer earthquakes, which reduces the sample size for statistical data fitting but improves confidence that all events above Mc are recorded, as shown in Figure 2). Thus, our preferred Mc is an averaged value between MAXC + Bootstrapping and MBS + Bootstrapping, as it balances maintaining sample size, and ensuring reliable event observation.

Table 1. Summary of results from the Woods Point regional seismicity study, organised by time period and magnitude type, based on frequency-magnitude distribution.

		Background Seismicity (2000 to 2021)		**Synthetic Background Seismicity I****	**Regional Background Seismicity I*****	**WPAS (2021 to 2024)**	
		M_L	M_W	M_L	M_W	M_L	M_W
Mc *(n*)*	MAXC	1 *(327)*	1.8 *(327)*	2.0~2.5	-	0.6 *(1349)*	1.5 *(1349)*
	MAXC+ Bootstrapping	0.90+/-0.24 *(272~416)*	1.71+/-0.18 *(272~384)*			0.61+/-0.06 *(1186~1349)*	1.50+/-0.02 *(1046~1349)*
	MBS	3.3 *(26)*	2.9 *(79)*			0.9 *(923)*	1.9 *(556)*
	MBS+ Bootstrapping	3.16+/-0.22 *(22~38)*	2.89+/-0.18 *(48~88)*			1.00+/-0.13 *(556~923)*	1.85+/-0.08 *(456~800)*
	Preferred Mc	2.03+/-0.23 *(93~170)*	2.3+/-0.18 *(131~197)*			0.80+/-0.1 *(923~1046)*	1.68+/-0.06 *(800~923)*
GR Law	Observed Catalogue	b=0.58+/-0.04,a=3.29	b=0.73+/-0.04,a=3.94	b=0.9, a=2.93	b =1.24 +/- 0.05	b=0.76+/-0.02,a=3.63	b=1.07+/-0.03,a=4.79

** Number of earthquakes in the catalogue greater or equal to Mc*

*** Leonard (2008) suggested a Mc value for Southeast Australia since 1995, identifying the magnitude threshold based on the linear relationship of the frequency-magnitude distribution. Regarding the a-value of the Gutenberg-Richter Law, Leonard's result indicates a value of 3.7 per century per 10,000 km² for Southeast Australia. As the a-value reflects regional seismicity and is influenced by both the time window and spatial domain, the smoothed a-value from Leonard's result, adjusted for our study domain (Background Seismicity from 2000 to 2021, WPAS region), is approximately 2.93. Given this adjustment, the smoothed values from Leonard's (2008) findings—b-value of 0.8 and a-value of 2.93—are referred to as the Synthetic Background Seismicity I for the WPAS region.*

**** Allen et al. (2023) calculated a b-value for the Eastern Australian Phanerozoic Accretionary Terranes region, based on a declustered catalogue. Further details can be found in NSHA 2023 by Allen et al. (2023).*

Note: The MAXC method for Mc estimation, along with bootstrap resampling, and the MLE method for b-value calculation, including b-value uncertainty, were implemented using code adapted from the

'Basic Statistical Seismology Tutorial' by Sullivan & Peng (2011).
*[*http://geophysics.eas.gatech.edu/people/bsullivan/tutorial/StatisticalSeismology.htm*].*

Table 1 also compares b-values calculated from the WPAS region with several other regional estimates. As discussed by Nava et al. (2017) and others, a smaller sample size (i.e. higher Mc) reduces the number of events available for b-value estimation, thereby affecting the fitting accuracy. Figure 2 shows the relationship between the b-value estimate and its uncertainty as a function of the chosen Mc, as calculated for the various methods in this study. The b-value is also significantly affected by the magnitude type (see Figure 3), due to the non-linear conversion between M_L and M_W (for the conversion equation, see Appendix 1 - Data Description, Equation S1: *https://github.com/Yunqi12/Data-Description-Methodology*. Additionally, Allen et al. (2020) suggested the non-linear conversion between M_L and M_W magnitudes.). Regardless of the preferred Mc and magnitude type, however, the WPAS b-values lie on the high side of the uncertainty range of b-values estimated from pre-mainshock background seismicity. In contrast, the b-values calculated from the 2012 Moe M_L aftershock sequence (e.g., 0.64+/-0.05) in southeast Australia (i.e., a proximal and geologically analogous setting to the WPAS) are lower than pre-mainshock background seismicity b-values (i.e., 0.77 to 0.88) (Hoult et al., 2021).

When comparing our results with other Australian studies of the G-R Law, we find that the pre-mainshock background seismicity b-value for M_L is lower than the value (i.e., 0.9) calculated for Southeast Australia by Leonard (2008). Similarly, our pre-mainshock background seismicity b-value for M_W is lower than the 1.24 +/- 0.05 suggested by Allen et al. (2023) for background seismicity in the Eastern Australian Phanerozoic Accretionary Terranes region. However, our b-values from the WPAS (ranging from 0.76 to 1.07) are consistent with Leonard (2008) but remain smaller than those reported by Allen et al. (2023). The discrepancy between our background seismicity b-value and those from Leonard (2008) and Allen et al. (2023) is likely due to the limited spatial and temporal extent of our pre-mainshock background seismicity model (2000 to 2021), resulting in a relatively small dataset (93 to 197 events). Attanayake et al. (2023) obtained a b-value for the offshore Gippsland Basin in Southeast Australia between 2009 and 2021 that ranges from 0.6 to 0.73 (using an Mc cutoff between M_L 0.7 and M_L 1.2) This estimate, based on the MLE method, is similar to our b-value for M_L background seismicity (0.58 +/- 0.04). However, Attanayake et al. (2023) used a larger sample size, ranging from 1145 to 4004 events, to calculate their b-value. Our b-value, similar to that of Attanayake et al. (2023), is more susceptible to sampling bias (e.g., limited temporal and spatial extent) and overfitting (Godano et al., 2014) compared to the b-value estimates from Leonard (2008) and Allen et al. (2023). This is due to the epistemic uncertainty in selecting the Mc value for b-value estimation, leading to two possibilities. Firstly, the low Mc chosen may influence the statistical fitting, potentially causing the MLE method to overfit small-magnitude seismicity, placing less emphasis on larger-magnitude events. This results in a lower b-value and an overestimation of predicted seismicity for large magnitudes. Secondly, shifting Mc to a higher magnitude reduces the sample size and increases the weight of large-magnitude events in the fitting. In this study, this approach raises the b-value and increases statistical fitting uncertainty, potentially leading to an overestimation of predicted seismicity for smaller-magnitude events.

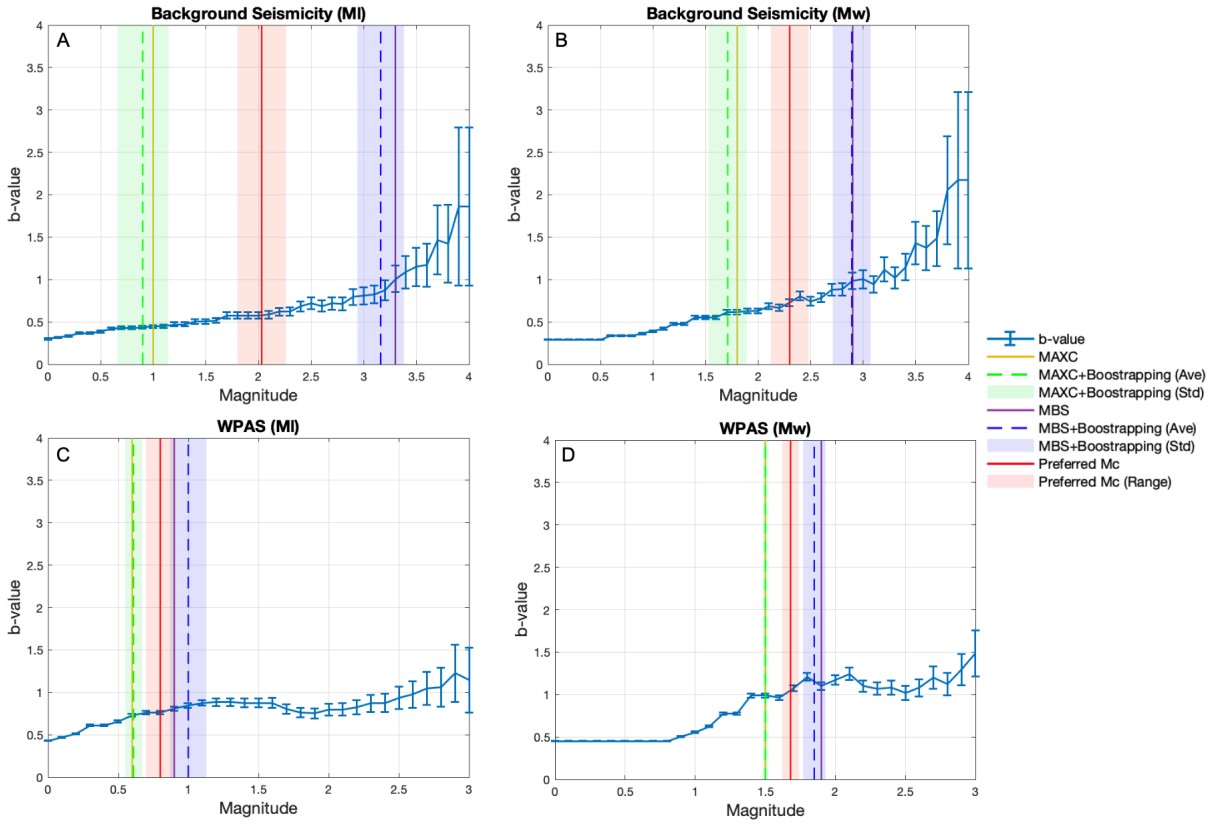

Figure 2. The b-value and its uncertainty vary with the selection of the Mc value. Figure A shows the variability of b-values with different Mc selections for pre-mainshock observed background seismicity in the M_L catalogue. Figure B shows the results for pre-mainshock observed background seismicity in the M_W catalogue. Figure C presents the results for the WPAS M_L catalogue, and Figure D presents the results for the WPAS M_W catalogue.

The Leonard (2008) a and b-values ("Synthetic Background Seismicity I"; Table 1) are obtained from $n>10^3$ earthquakes in a >100 yr duration regional catalogue (Southeast Australia) spanning changes in seismic network characteristics and associated uncertainties in M_L and Mc. As such there are numerous epistemic uncertainties in scaling the spatiotemporal characteristics of the Synthetic Background Seismcity I model to estimate a background seismicity rate for the smaller WPAS region and shorter sampling window (i.e., 2000 to 2021; Table 1). Theoretically, the longer duration and larger area of the Synthetic Background Seismicity I could reduce sampling biases associated with temporal and spatial variations in seismicity (i.e., 'smoothing'), but the assumption that regional seismicity can be scaled to estimate a background rate for a specific sub-region is epistemically uncertain. Seismicity rates for the WPAS region estimated from Leonard's b-value (0.9) and smoothed seismicity a-value scaled to the WPAS region (a-value = 2.93) are lower than the observed pre-mainshock seismicity rates for the same region ("Background Seismicity 2000 to 2021 M_L catalogue, Figure 4A). The Background Seismicity 2000 to 2021 M_L catalogue b-value (0.58) and a-value (3.29) suggest a higher potential productivity of small-magnitude events (below the Mc cutoff) than observed (i.e., missing events at $M_L<2$). There is epistemic uncertainty regarding whether locally observed pre-mainshock background seismicity (i.e., the G-R Law parameters calculated in this study) or smoothed regional seismicity (i.e., Leonard, 2008) more accurately represents the background seismicity rate for the WPAS region. The b-value of the WPAS region is sensitive to Mc selection, catalogue variations (e.g., differences in catalogue source), and spatial-temporal variability (Godano et al., 2014). Additionally, the observed seismicity is affected by epistemic and sampling errors (e.g., limited spatial and temporal windows), which may induce uncertainty in b-value calculation and Mc selection. Given these sensitivities, we calculate the preferred G-R relationship parameters for the WPAS region (Table 1) during the

pre-mainshock stage, by averaging the frequency–magnitude relationship for Leonard's results with our study. The calculated pre-mainshock background seismicity G-R Law parameters from this study and Leonard (2008) with the observed earthquake productivity in the WPAS region.

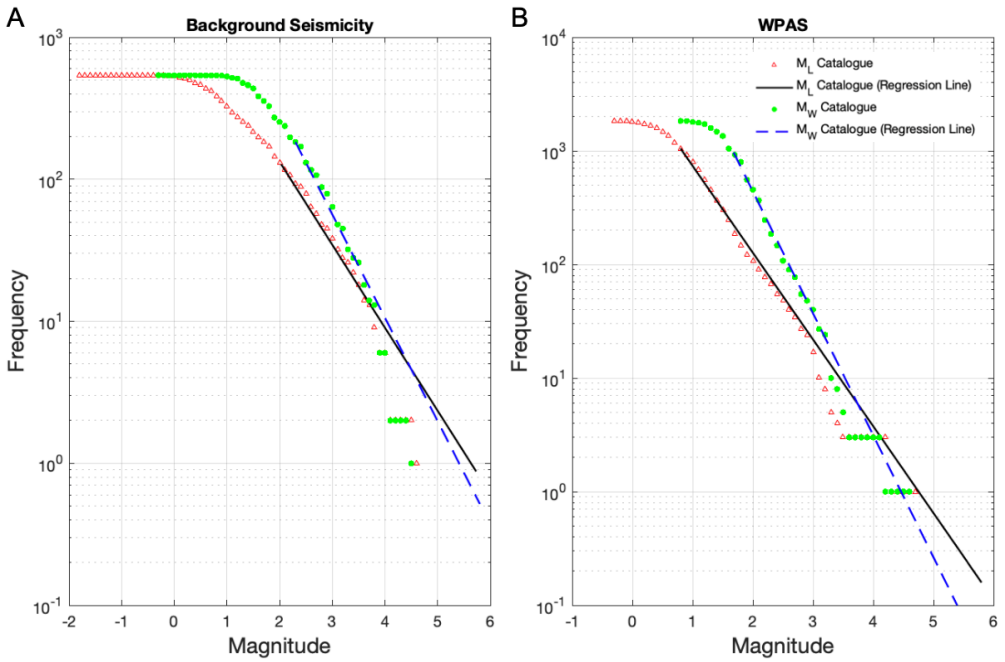

Figure 3. Pre-mainshock observed background seismicity and WPAS G-R Law magnitude-frequency distribution, based on the preferred Mc values listed in Table 1, for both M_L and M_W catalogues.

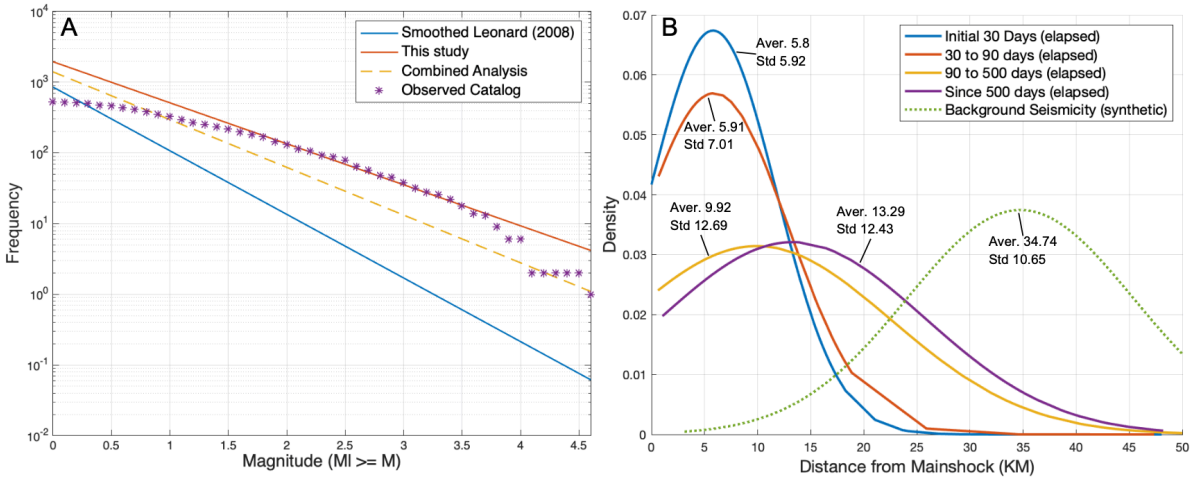

Figure 4. A) Frequency-Magnitude Distribution, including Leonard's (2008) smoothed results (Synthetic Background Seismicity I), the model from this study, which is based on observed pre-mainshock background seismicity based on M_L Catalogue, and the combined result from Leonard's and the observed pre-mainshock background seismicity. B) Distance Probability Distribution Function (pdf) from the mainshock to the events observed in the Woods Point region across different periods: (1) the first 30 days following the mainshock, (2) from 30 to 90 days following the mainshock, (3) from 90 to 500 days following the mainshock, (4) from 500 days after the mainshock until 7th August 2024, and (5) Synthetic Background Seismicity II.

4.2 Modified Omori's Law

The Modified Omori's Law was calculated based on the preferred Mc for WPAS (Mc = 0.8 for M_L, and Mc = 1.68 for M_W, see Table 2). The c-value for both magnitude types (M_L and M_W) is 0, indicating that the aftershock sequence follows a power-law decay immediately after the

mainshock. However, this parameter is sensitive to the selection of Mc, typically decreasing as Mc increases (Shcherbakov et al., 2012). The k-value, which reflects aftershock productivity and is scaled according to the mainshock's magnitude (Helmstetter & Sornette, 2003), differs between the M_L and M_W catalogues (64.8 for M_L and 56.3 for M_W), primarily due to variations in Mc. The p-value for WPAS for both M_L and M_W is 0.84 and 0.83, respectively. The global average p-value for aftershock sequences is around 1.1 (Utsu et al., 1995). Our p-value, which is less than 1, suggests a relatively slow decay rate of aftershock sequences compared to the global average, including a slower decay than some other sequences in Australia, such as Tennant Creek (1988, M_W 6.2, M_W 6.3 and M_W 6.6, p = 0.96) (Ebel et al., 2000) and Meckering (1968, M_W 6.6, p = 1) (Ebel, 2009).

Table 2. Modified Omori's Law Parameters derived from the WPAS, and the modelled WPAS duration.

		M_L		**M_W**	
		MLE Method	Bayesian Method	MLE Method	Bayesian Method
		c=0, k=64.81, p=0.84	c=0, k=64.84, p=0.84	c=0, k=56.25, p=0.83	c=0, k=56.25, p=0.83
Aftershock Anticipated Duration (days)	Smoothed Leonard (2008)	14759.2	14767.3	-	-
	Model based on Observed Background Seismicity (This study)	2722	2723.5	3590.5	3590.5
	Combined Result	4958.2	4960.9	-	-

Note: The Ogata method and Bayesian method for Modified Omori's Law calculation were implemented using code adapted from "Seishimi" by Liu (2022) [https://github.com/yuankailiu/Seishimi].

4.3 Modelled Duration of the WPAS

As of 7th August 2024 (UTC+0), the observed current seismicity rate in the WPAS region (eqs ≥ Mc) is above background rates (Figure 5A and B). WPAS seismicity rates could reach background rates between ca. 2700 days (7.4 years) to ca. 14760 days (40.4 years) depending on the fitting method and background seismicity model used (Table 2). An epistemically uncertain assumption central to these estimations is that the WPAS continues to decay at the modelled rate.

The spatial distribution of observed seismicity in the WPAS region is still clustered proximal to the Woods Point mainshock hypocentre (average distance ≈ 13 km) and is distinct from a calculated synthetic background seismicity distribution (Figure 4B). The observed monthly seismic moment release from seismicity in the WPAS region is still higher than the 68% confidence interval of the monthly seismic moment release observed during the pre-mainshock background seismicity period (Figure 5C and D). A M_L 4.2 aftershock occurred on 6th August 2024. Collectively, these aspects suggest the WPAS is still continuing.

The apparent duration of aftershock sequences (i.e., the post-mainshock time period in which aftershocks dominate seismicity) is strongly dependent on mainshock magnitude and background seismicity rate (Hainzl et al., 2016). Mc is also a relevant parameter. The modelled duration of an aftershock sequence with analogous characteristics to the WPAS (mainshock Mw 5.9 to 6.0; background seismicity average rate ca. 0.02 to 0.002 eq/day; Mc ≈2) based on global events ranges from ca. 5.5 to > 60 yrs (Hainzl et al., 2016). From this perspective, the WPAS sequence currently adheres well to expectations of sequence duration, given the wealth of uncertainties inherent in estimations on this nature.

4.4 Distribution of seismic moment release from the WPAS relative to the rupture plane

The rupture planes fitted from the WPAS in this study shows similar results to the two published sources of the rupture plane (Table 3B). The high double couple of the mainshock (>80% - Mousavi et al., 2023) and good statistical fit of a sub-vertical plane to the WPAS data, suggests a simple mainshock source fault. However, the complex behaviour of aftershock sequences in SCRs introduces additional challenges. For instance, interactions within a complex fault system (Liu & Stein, 2016) may cause deviations from the expected geometric distribution of the rupture plane. These deviations can complicate efforts to statistically fit aftershocks to the rupture plane model, making interpretation and accuracy more difficult.

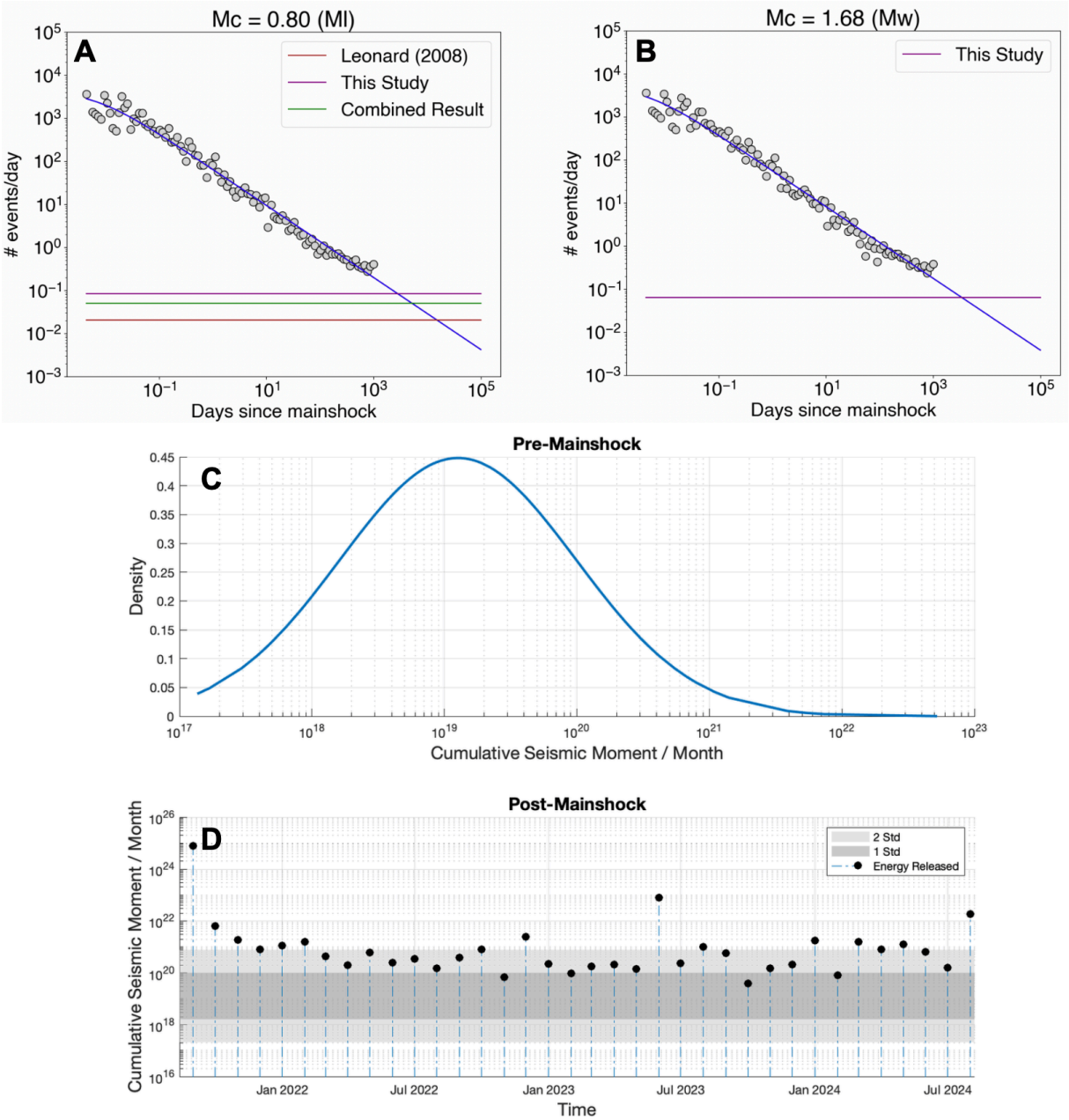

Figure 5. Comparison of post-mainshock seismicity level with observed pre-mainshock seismicity level. Figures A and B compare the current seismicity rate with the Synthetic Background Seismicity II. Figures C and D show the seismic moment released in the Woods Point region per month (within a 50 km radius from the mainshock hypocenter). Figure C displays the normal distribution of seismic moment released from the observed seismicity during the pre-mainshock period, while Figure D illustrates the monthly cumulative seismic moment release since the mainshock, compared to the pre-mainshock level. The

shaded area representing one standard deviation from the pre-mainshock cumulative seismic moment distribution includes 68% of the background seismicity, and the area representing two standard deviations includes 95% of the pre-mainshock level. Note: Figures A and B were obtained using code adapted from "Seishimi" by Liu (2022) [https://github.com/yuankailiu/Seishimi].

Table 3. Table A summarise source models reported by various sources. Table B summarises fault planes reported by various researchers, alongside the results obtained from this study.

Table 3-A

Source	Hypocenter			Centroid			Nodal Planes		
	Longitude (°)	Latitude (°)	Depth (Km)	Longitude (°)	Latitude (°)	Depth (Km)	Stike (°)	Dip (°)	Rake (°)
GA	146.35	-37.49	10	146.27	-37.44	18	172	83	0
							82	90	173
GFZ	-	-	-	146.4	37.51	19	172	76	-11
							256	79	-166
Global CMT	-	-	-	146.27	-37.47	18.1	353	76	6
							262	84	166
Mousavi et al. (2023)	146.39	-37.53	16.8	146.4	-37.5	15	348	87	13
							258	77	177
USGS	146.35	-37.49	12	146.36	-37.49	21.5	351	84	15
							259	75	174

Note: Adapted from Mousavi et al. (2023), Table 3A. GFZ refers to GeoForschungsZentrum, Global CMT to the Global Centroid Moment Tensor, and USGS to the U.S. Geological Survey.

Table 3-B

Source	Fault Plane						
	Strike (°)	Dip (°)	Length (Km)	Width (Km)	Min. Depth (Km)	Max. Depth (Km)	Aver. Slip (m)
Mousavi et al. (2023)	348 ± 2	87	-	~8*	11	19	-
Quigley et al. (2021)	350	85	8	9	(ca.) 4	(ca.) 13	-
Preferred Fault Plane (This study)	352.81 +/- 3.2	85.50E +/- 2.97	4.8 ~ 6.6 (aver. 5.96)	6.77 ~ 9.31 (aver. 7.55)	7.63 ~ 8.96 (aver. 8.36)	14.83 ~ 17.82 (aver. 15.88)	0.59

** An approximate calculation based on the depth range of the rupture plane and the dip angle provided by Mousavi et al. (2023)*

When we then compare cumulative seismic moment release with distance from all the fault planes fitted to WPAS in this study, we find that the maximum curvature of the moment release is within 1.5 km of the fault planes. We define this area as the on-fault aftershock zone, where the amount of seismic moment released accumulates rapidly due to the clustering of aftershocks caused by intense displacement and slip near the rupture plane (Yukutake & Iio, 2017). When considering distance greater than 1.5 km from the fault planes, the seismic moment release rate decays until it reaches 100%. This is with the exception of the M_L 4.2 aftershock in September 2021 (approximately 18 minutes after the mainshock) and the M_L 4.7 aftershock in June 2023 which are interpreted to be off-fault aftershocks since they occurred more than 1.5 km from the mainshock rupture plane. The M_L 4.2 earthquake (which occurred on the 6th of August 2024) is interpreted to be an on-fault aftershock because it occurred less than 1.5 km from the mainshock rupture plane (Figure 6). However, uncertainty in event locations may affect the boundary between on-fault and off-fault aftershocks. By 7th August 2024, the on-fault aftershock zone accounted for 29.4% of the total seismic moment released from the WPAS seismicity (i.e., 10 km from the rupture plane on each side).

Estimates of earthquake damage zone widths range from 200 to 250m, as observed in the 1992 M_W 7.3 Landers earthquake (Peng et al., 2003), the 2010 M_W 7.1 Darfield earthquake (Li

et al., 2014), and the Parkfield segment of the San Andreas Fault (Lockner et al., 2011). Our inferred 1.5 km half-width of the Woods Point mainshock fault zone, determined from the maximum curvature of moment release (Figure 6), is consistent with half-width estimates of seismicity fall-offs from strike-slip earthquakes on slow-slip rate faults in California (e.g., 0.8 to 1 km; Perrin et al., 2021). Considering potential complicating factors, such as epistemic uncertainties in aftershock locations, we estimate the total width of the dilatant damage zone associated with volumetric strains in the mainshock fault zone to be approximately 3 km, with secondary faulting (i.e., large aftershocks on distinct faults) extending to distances greater than 5 km from the mainshock fault.

4.5 Largest Aftershock of the WPAS

As of 7th August 2024, the largest recorded aftershock in the WPAS was a M_L 4.7 earthquake that occurred in June 2023. The largest aftershock, with a magnitude 1.1 lower than the mainshock, occurred approximately 1.8 years (646 days) after the mainshock. According to Modified Bath's Law (Shcherbakov & Turcotte, 2004), the expected largest aftershock magnitude for a M_L 5.8 mainshock is a M_L 4.7, which is consistent with the WPAS. However, according to Geoscience Australia Online, the 2021 Woods Point mainshock is listed as M_L 6.0 (accessed on 9th November 2024), while NSHA23 (Allen et al., 2023) revises the mainshock magnitude to M_L 6.3. Based on the reference magnitude differences from Modified Bath's Law, the expected largest aftershock would be M_L 4.9 and M_L 5.2, respectively.

Typically, the median time interval between the mainshock and the largest aftershock is 3 days, with the largest aftershock more likely to occur earlier in the sequence (Tahir et al., 2012). Ebel (2009) calculated a 40% probability that the largest aftershock in SCRs would occur within 5 days of the mainshock, a 70% probability within 60 days, and a 30% probability greater than 60 days. The 646-day interval between the mainshock and the largest aftershock in the WPAS represents a delayed occurrence compared to other SCR aftershock sequences. Additionally, the distance of the largest observed aftershock at the WPAS region is approximately 4.6 to 5.1 km from the mainshock rupture plane. The presence of the largest aftershock occurring greater than 5 km from the mainshock is consistent with other global aftershock sequences, including the M_W 7.3 1992 Landers earthquake, USA, where the largest aftershock (M_W 6.2) occurred approximately 30 km west of the mainshock (Hauksson et al., 1993)., and the M_W 7.1 2010 Darfield earthquake, NZ, where the largest aftershock (M_W 6.1) occurred approximately 40 km east of the mainshock (Li et al., 2014).

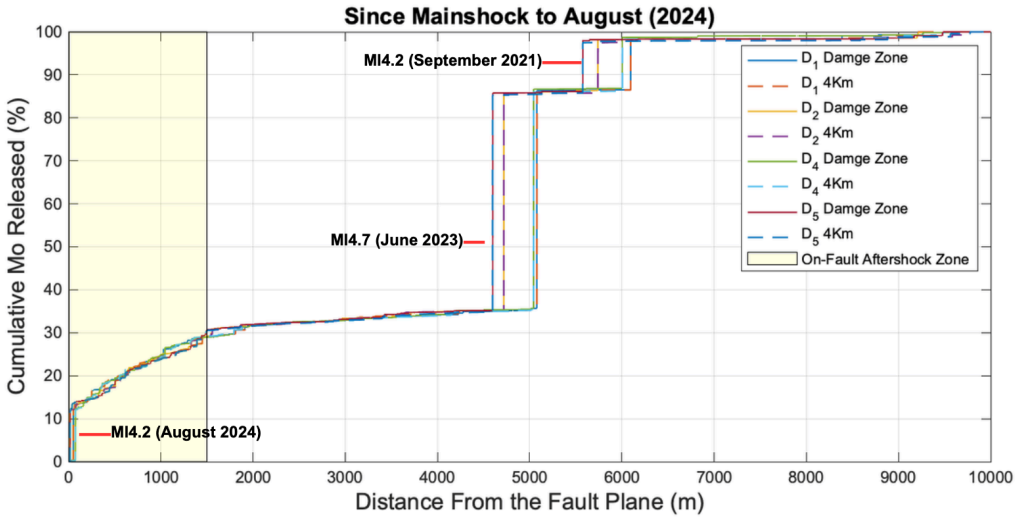

Figure 6. The relationship between the seismic moment released from the WPAS and their distance from the fault planes obtained in this study. This figure uses the catalogue of aftershocks observed from the mainshock until 7th August 2024 within a 20 km radius from the mainshock's hypocenter. The spatial distribution of seismic moment was analysed based on the 4 rupture-plane locations determined in this study. The maximum curvature zone for the Woods Point earthquake is approximately 1.03 km to 1.45

km from the fault plane, rounded to a 1.5 km cutoff zone, highlighted in yellow. D1, D2, D4, and D5 represent the subdatasets. For more information about the fault plane estimated from this study, please refer to Appendix 2, please visit https://github.com/Yunqi12/Data-Description-Methodology.

5 Conclusions

1. b-value Estimation: The WPAS b-value is 0.76 (for M_L catalog) and 1.07 (for M_W catalog). This is consistent with the pre-mainshock background seismicity b-value of 0.9 (Leonard, 2008), but lower than the regional b-value of 1.24 (Allen et al., 2023). The estimated b-value for the pre-mainshock observed background seismicity is lower, ranging from 0.58 to 0.73; this estimate is likely plagued by the small number of events, potential for sampling bias associated with small space and time window, magnitude types and conversions, and a suite of epistemic uncertainties.
2. Modelled Duration of Aftershock Sequence: The estimates of WPAS duration could range from 7 to more than 40 years. As of 7th August 2024 (approximately 3 years after the mainshock), we determined that the WPAS could continue for several decades before the seismicity rates align with pre-mainshock background levels. The spatial distribution of WPAS does not yet conform to the synthetic background seismicity distribution, and monthly seismic moment release is still above pre-mainshock levels. In addition, the WPAS has a slower decay rate (i.e., Modified Omori's law *p*-value of 0.83~0.84) than the global average (e.g., p ≈ 1.1; Utsu et al., 1995).
3. Rupture Plane Fitting: The fault plane identified from the WPAS, aligns with published focal mechanisms and waveform analyses, showing a strike of 352.81° +/- 3.2° and a near-vertical dip of 85.50°E +/- 2.97°. The fault plane's dimensions range from 4.8 to 6.6 km in length and 6.77 to 9.31 km in down-dip rupture width, with rupture depths varying from 7.63 to 17.82 km.
4. On-fault Aftershock Zone: We delineate the on-fault aftershock zone to extend 1.5 km on each side of the fault plane. We find this zone accounts for 29.4% of the total seismic moment released from near-source seismicity, including the M_L 4.2 earthquake in August 2024. The two other largest aftershocks, M_L 4.7 in June 2023 and M_L 4.2 in September 2021, are considered off-fault aftershocks.
5. Delay of Largest Aftershock: The expected largest aftershock, around M_L 4.7 (using Modified Bath's law), matches the observed largest aftershock in June 2023. However, the 1.8-year interval between the mainshock and the largest aftershock is significantly longer than in other SCR aftershock sequences, as statistical analysis shows that in 70% of cases, the largest aftershocks in SCRs occur within 60 days (Ebel, 2009).

6 Acknowledgements

We thank Abraham Jones, Januka Attanayake, Trevor Allen, Dan Sandiford, Yuxiang (Gideon) Tang and Dee Ninis for scientific discussions relating to this work. This research was funded by the Australian Government National Emergency Agency (NEMA) Disaster Ready Fund (Project DRF 40204) and by AuScope (Projects 3.127, 3.128) via the National Collaborative Research Infrastructure Strategy (NCRIS).

7 References

Aki, K. (1965). Maximum likelihood estimate of b in the formula log10N = a - bm and its confidence limits. *Bulletin of Earthquake Research, 43*, 237-239.

Allen, T. I., Griffin, J. D., Clark, D. J., Cummins, P. R., Ghasemi, H., & Ebrahimi, R. (2023). The 2023 National Seismic Hazard Assessment for Australia.

Allen, T. I., Griffin, J. D., Leonard, M., Clark, D. J., & Ghasemi, H. (2020). The 2018 national seismic hazard assessment of Australia: Quantifying hazard changes and model uncertainties. *Earthquake Spectra*, *36*(1_suppl), 5-43.

Attanayake, J., Jones, A., Gibson, G., & Sandiford, M. (2023). Pre-commercial baseline passive seismic monitoring around CarbonNet's Pelican Site in the offshore Gippsland Basin, Victoria—The first five years. *International Journal of Greenhouse Gas Control*, *128*, 103962.

Cao, A., & Gao, S. S. (2002). Temporal variation of seismic b-values beneath northeastern Japan island arc. *Geophysical Research Letters, 29*(9), 48-1-48-3.

Ebel, J. E. (2009). Analysis of aftershock and foreshock activity in stable continental regions: Implications for aftershock forecasting and the hazard of strong earthquakes. *Seismological Research Letters*, *80*(6), 1062-1068.

Ebel, J. E., Bonjer, K. P., & Oncescu, M. C. (2000). Paleoseismicity: Seismicity evidence for past large earthquakes. *Seismological Research Letters*, *71*(2), 283-294.

Efron, B., & Tibshirani, R. J. (1994). *An introduction to the bootstrap*. Chapman and Hall/CRC.

Freed, A. M. (2005). Earthquake triggering by static, dynamic, and postseismic stress transfer. *Annual Review of Earth and Planetary Sciences, 33*(1), 335-367.

Godano, C., Lippiello, E., & de Arcangelis, L. (2014). Variability of the b value in the Gutenberg–Richter distribution. *Geophysical Journal International*, *199*(3), 1765-1771.

Hainzl, S., Christophersen, A., Rhoades, D., & Harte, D. (2016). Statistical estimation of the duration of aftershock sequences. *Geophysical Journal International*, *205*(2), 1180-1189.

Hauksson, E., Jones, L. M., Hutton, K., & Eberhart-Phillips, D. (1993). The 1992 Landers earthquake sequence: Seismological observations. *Journal of Geophysical Research: Solid Earth*, *98*(B11), 19835-19858.

Helmstetter, A., & Sornette, D. (2003). Importance of direct and indirect triggered seismicity in the ETAS model of seismicity. *Geophysical Research Letters*, *30*(11).

Holschneider, M., Narteau, C., Shebalin, P., Peng, Z., & Schorlemmer, D. (2012). Bayesian analysis of the modified Omori law. *Journal of Geophysical Research: Solid Earth, 117*(B6).

Hoult, R., Allen, T., Borleis, E., Peck, W., & Amirsardari, A. (2021). Source and attenuation properties of the 2012 Moe, southeastern Australia, earthquake sequence. *Seismological Society of America, 92*(2A), 1112-1128.

Jordan, T.H., Chen, Y.T., Gasparini, P., Madariaga, R., Main, I., Marzocchi, W., Papadopoulos, G., Sobolev, G., Yamaoka, K. & Zschau, J. (2011). Operational earthquake forecasting: State of knowledge and guidelines for utilization. *Annals of Geophysic*s, 54(4), pp.315-391.

Leonard, M. (2008). One hundred years of earthquake recording in Australia. *Bulletin of the Seismological Society of America, 98*(3), 1458-1470.

Li, Q., Liu, M., & Stein, S. (2009). Spatiotemporal complexity of continental intraplate seismicity: Insights from geodynamic modeling and implications for seismic hazard estimation. *Bulletin of the Seismological Society of America*, *99*(1), 52-60.

Li, Y. G., De Pascale, G. P., Quigley, M. C., & Gravley, D. M. (2014). Fault damage zones of the M7. 1 Darfield and M6. 3 Christchurch earthquakes characterized by fault-zone trapped waves. *Tectonophysics*, *618*, 79-101.

Liu, M., & Stein, S. (2016). Mid-continental earthquakes: Spatiotemporal occurrences, causes, and hazards. *Earth-Science Reviews, 162*, 364-386.

Liu, Y. (2022). *Seishimi*. GitHub. https://github.com/yuankailiu/Seishimi

Lockner, D. A., Morrow, C., Moore, D., & Hickman, S. (2011). Low strength of deep San Andreas fault gouge from SAFOD core. *Nature*, *472*(7341), 82-85.

Mignan, A., & Woessner, J. (2012). Estimating the magnitude of completeness for earthquake catalogues. *Community Online Resource for Statistical Seismicity Analysis*. https://doi.org/10.5078/corssa-00180805. Available at http://www.corssa.org

Mousavi, S., Hejrani, B., Miller, M. S., & Salmon, M. (2023). Hypocenter, fault plane, and rupture characterization of Australian earthquakes: Application to the September 2021 Mw 5.9 Woods Point earthquake. *Seismological Society of America, 94*(4), 1761-1774.

Nava, F. A., Márquez-Ramírez, V. H., Zúñiga, F. R., Ávila-Barrientos, L., & Quinteros, C. B. (2017). Gutenberg-Richter b-value maximum likelihood estimation and sample size. *Journal of Seismology*, *21*, 127-135.

Ninis, D., Borleis, E., Quigley, M., Peck, W., & Wilcox, J. (2021, November). The Mw 5.9 Woods Point earthquake and aftershock sequence. In *Australian Earthquake Engineering Society 2021 Virtual Conference* (pp. 25-26).

Ogata, Y. (1983). Estimation of the parameters in the modified Omori formula for aftershock frequencies by the maximum likelihood procedure. *Journal of Physics of the Earth, 31*(2), 115-124.

Ozawa, S., & Ando, R. (2021). Mainshock and aftershock sequence simulation in geometrically complex fault zones. *Journal of Geophysical Research: Solid Earth*, *126*(2), e2020JB020865.

Peng, Z., Ben-Zion, Y., Michael, A. J., & Zhu, L. (2003). Quantitative analysis of seismic fault zone waves in the rupture zone of the 1992 Landers, California, earthquake: evidence for a shallow trapping structure. *Geophysical Journal International*, *155*(3), 1021-1041.

Perrin, C., Waldhauser, F., & Scholz, C. H. (2021). The shear deformation zone and the smoothing of faults with displacement. *Journal of Geophysical Research: Solid Earth*, *126*(5), e2020JB020447. https://doi.org/10.1029/2020JB020447

Quigley, M. C., Hughes, M. W., Bradley, B. A., van Ballegooy, S., Reid, C., Morgenroth, J., Horton, T., Duffy, B., & Pettinga, J. R. (2016). The 2010–2011 Canterbury earthquake sequence: Environmental effects, seismic triggering thresholds and geologic legacy. *Tectonophysics*, 672, 228-274.

Quigley, M., Pascale, A., Clark, D., & Allen, T. (2021). Wednesday 22 September 2021 Mw 5.9 Woods Point earthquake – Information Sheet. Accessed at: https://learningfromearthquakes.org/2021-09-22-australia/images/2021_09_22-australia/pdfs/REPORT_EQ_27_SEPT_2021_short.TA.pdf

Shcherbakov, R., & Turcotte, D. L. (2004). A modified form of Bath's law. *Bulletin of the Seismological Society of America, 94*(5), 1968-1975.

Shcherbakov, R., Nguyen, M., & Quigley, M. (2012). Statistical analysis of the 2010 MW 7.1 Darfield Earthquake aftershock sequence. *New Zealand Journal of Geology and Geophysics*, *55*(3), 305-311.

Shi, Y., & Bolt, B. A. (1982). The standard error of the magnitude-frequency b value. *Bulletin of the Seismological Society of America, 72*(5), 1677-1687.

Stein, S., & Liu, M. (2009). Long aftershock sequences within continents and implications for earthquake hazard assessment. *Nature, 462*(7269), 87-89. https://doi.org/10.1038/nature08502

Sullivan, B., & Peng, Z. (2011). *Basic statistical seismology tutorial*. http://geophysics.eas.gatech.edu/people/bsullivan/tutorial/StatisticalSeismology.htm

Tahir, M., Grasso, J. R., & Amorese, D. (2012). The largest aftershock: How strong, how far away, how delayed?. *Geophysical Research Letters*, *39*(4).

Toda, S., & Stein, R. S. (2018). Why aftershock duration matters for probabilistic seismic hazard assessment. Bulletin of the Seismological Society of America, 108(3A), 1414-1426.

Utsu, T. (1965). A method for determining the value of b in a formula log n= a-bM showing the magnitude frequency relation for earthquakes. *Geophys. Bull. Hokkaido Univ.*, *13*, 99-103.

Utsu, T., Y. Ogata, & R. S. Matsu'ura (1995), The centenary of the Omori formula for a decay law of aftershock activity, *J. Phys. Earth*, **43**(1), 1–33.

Wiemer, S., & Wyss, M. (2000). Minimum magnitude of complete reporting in earthquake catalogues: examples from Alaska, the Western United States, and Japan. *Bulletin of the Seismological Society of America, 90*(4), 859–869.

Woessner, J., & Wiemer, S. (2005). Assessing the quality of earthquake catalogues: Estimating the magnitude of completeness and its uncertainty. *Bulletin of the Seismological Society of America, 95*(2), 684-698.

Wyss, M., Hasegawa, A., Wiemer, S., & Umino, N. (1999). Quantitative mapping of precursory seismic quiescence before the 1989, M 7.1 off-Sanriku earthquake, Japan. *Annals of Geophysics, 42*(5).

Yukutake, Y., & Iio, Y. (2017). Why do aftershocks occur? Relationship between mainshock rupture and aftershock sequence based on highly resolved hypocenter and focal mechanism distributions. *Earth, Planets and Space*, *69*, 1-15.